

pubs.acs.org/JPCL Letter

From Light to Dark: Dancing with Electrons in Colloidal 2D MoS₂ Nanosheets

Bo-An Chen, Nathaniel L. Dominique, Anthony Kipkorir, Jon P. Camden, Sylwia Ptasinska, and Prashant V. Kamat*



Cite This: J. Phys. Chem. Lett. 2024, 15, 4920-4927



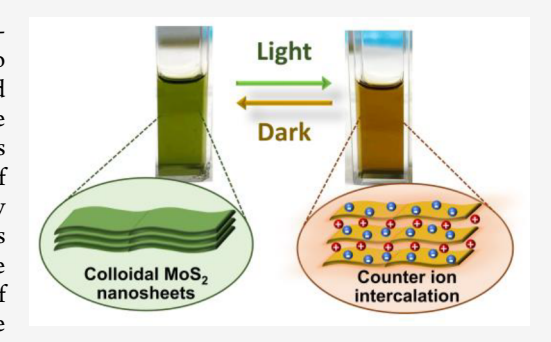
ACCESS I

Metrics & More

Article Recommendations

s Supporting Information

ABSTRACT: Extending the lifetime of photogenerated electrons in semi-conductor systems is an important criterion for the conversion of light into storable energy. We have now succeeded in storing electrons in a photoirradiated colloidal molybdenum disulfide (MoS_2) suspension, showcasing its unique reversible photoresponsive behavior. The dampened A and B excitonic peaks indicate the accumulation of photogenerated electrons and the minimization of interactions between MoS_2 interlayers. The stored electrons were quantitatively extracted by titrating with a ferrocenium ion in the dark, giving ca. 0.2 electrons per MoS_2 formula unit. The emergence of the photoinduced A_{1g}^* Raman mode and the decrease in zeta potential after irradiation suggest intercalation of counterions to maintain overall charge balance upon electron storage. These results provide insights into the mechanism of photogenerated electron storage



in 2D materials and pave the way for the potential application of colloidal 2D materials in electron storage.

TMDs) have gained attention metal dichalcogenides (2D TMDs) have gained attention in recent years because of their interesting electronic, optical, and catalytic properties compared to their bulk counterparts. Among the TMD compounds, the intrinsic semiconducting nature of 2H phase MoS₂ makes it a promising material for various applications, ranging from electronics to optoelectronics. Additionally, atomically thin MoS₂ exhibits a unique indirect-to-direct bandgap transition as the number of layers reduces to a monolayer with a layer-dependent bandgap energy between 1.3 and 1.8 eV. The ability to engineer MoS₂ with cocatalysts at the nanoscale level enables the enhancement of light absorption, charge separation, and catalytic activity, making MoS₂ a promising candidate for visible-light harvesting. 11–14

Owing to the van der Waals layered crystal structure of MoS₂, with a layer spacing of approximately 0.65 nm, it is possible to incorporate guest species between the layers via intercalation without interrupting any chemical bonds. Chemical or electrochemical intercalation of MoS₂ has been extensively utilized to prepare colloidal MoS₂ nanosheets through liquid-phase exfoliation. By precisely controlling the intercalation chemistry, phase-pure semiconducting 2H-MoS₂ nanosheets can be exfoliated, further demonstrating high-quality solution-processability of this class of 2D material. Subsequently, these colloidal MoS₂ nanosheets can be readily deployed in electronic device fabrication using simple, scalable and cost-effective deposition techniques, i.e., spin-coating or inkjet-printing. ^{21–23} While much of the research on exfoliated colloidal MoS₂ has predominantly focused on electronic and optoelectronic applications, there remains a

notable gap in the exploration of its potential in solar energy harvesting.

Colloidal MoS₂, as a photosensitizer, has been explored for photocatalytic water splitting, ¹¹ solar cell, ²⁴ and degradation of pollutants. ²⁵ By employing colloidal MoS₂, Yu et al. ²⁶ were able to design large-area bilayer thin films by depositing MoS₂ on organic semiconductor (perylene-diimide). The *p-n* heterojunction facilitated interfacial charge transfer, resulting in a 6-fold increase in photocurrent compared to that of bare MoS₂. In this study, we synthesized a colloidal MoS₂ nanosheet via electrochemical intercalation-assisted liquid phase exfoliation. Curiously, the as-synthesized colloidal MoS₂ nanosheets undergo a color transformation from green to brown upon irradiation and recover back to their original state in the dark. This study aims to explore the underlying mechanism of this photoinduced color transformation by using UV—vis absorption, Raman spectroscopy and Zeta potential measurements.

Colloidal MoS_2 nanosheet suspensions were prepared using a previously established procedure^{12,21} (details are presented in the Supporting Information). Briefly, a crystal MoS_2 was subjected to electrochemical intercalation using tetrahepty-lammonium (THA⁺) as an intercalating bulky cation in a two-

 Received:
 February 12, 2024

 Revised:
 April 20, 2024

 Accepted:
 April 25, 2024

 Published:
 April 29, 2024





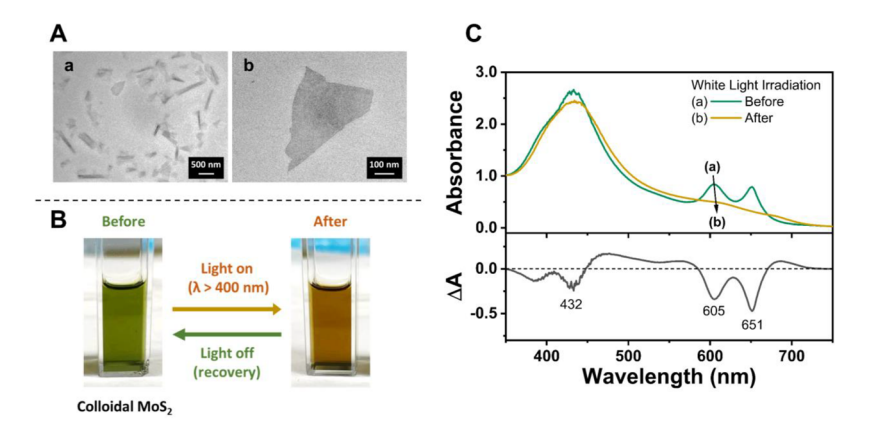


Figure 1. (A) TEM images of as-prepared colloidal MoS_2 nanosheet suspensions at two different magnifications. Scale bar: (a) 500 and (b) 100 nm. (B) Schematic illustration of the color change in colloidal MoS_2 nanosheet suspensions (in PVP/IPA under ambient condition) before and after white light irradiation. The color of MoS_2 changes from green to brown upon white light exposure and reverses back in the dark. (C) Absorption spectra of colloidal MoS_2 nanosheet suspensions before and after white light irradiation along with the corresponding difference in absorbance. The arrow represents the absorbance trends upon white light exposure (irradiation time: 30 min, light source: $\lambda > 400$ nm, 100 mW/cm²).

electrode cell. The suspension was subsequently sonicated in a polyvinylpyrrolidone/dimethylformamide (PVP)/DMF) solution to obtain a dark green dispersion of MoS₂ nanosheets. The dispersion was then centrifuged at 8000 r.p.m. for 30 min to remove excess PVP. After discarding the supernatant, the residue was redispersed in isopropyl alcohol (IPA), to obtain a light green MoS₂ dispersion. This suspension was further centrifuged at 8,000 r.p.m. for 30 min to remove large aggregates, and the colloidal MoS₂ (few layer) nanosheets were collected from the supernatant. In contrast to the black appearance of bulky or metallic MoS₂ crystals, the transparent light green color observed in the collected supernatant suggests the dispersion of a few-layers semiconducting MoS₂ nanosheets. Figure 1A shows TEM images of MoS₂ nanosheets obtained from this experimental procedure.

The photoresponsive behavior of the colloidal MoS₂ nanosheet suspensions was examined by exposing them to white light irradiation ($\lambda > 400$ nm). During irradiation, we observed color changes of the suspension, transitioning from light green to brown. When the light was turned off, it reverted into the original light green color. These observed color changes are shown in Figure 1B. We corroborated this light induced color change by recording absorption spectra of the as-prepared colloidal MoS₂ nanosheet suspensions before and after white light irradiation (Figure 1C). The absorption spectrum of MoS₂ before irradiation reveals three characteristic excitonic peaks at about 650, 610, and 430 nm, arising from the A, B, and C exciton transitions, respectively. The A and B exciton peaks are associated with the spin-orbit splitting of the valence band edge at the K point of the Brillouin zone, 9,27,28 while the C exciton peak is attributed to the band nesting between the Γ and Λ positions of the Brillouin zone.²⁹ These three distinct peaks collectively confirm the existence of the semiconducting 2H phase of MoS₂ nanosheets dispersed in the suspension.

Upon white light irradiation ($\lambda > 400$ nm), the absorbance of the A and B excitonic peaks decrease, transforming into a broad spectral feature (Figure 1C, trace b). The spectral feature of the C exciton band, on the other hand, shows only a small decrease during the photoirradiation. When we present the spectral changes in the form of difference absorption spectra (bottom trace in Figure 1C), we can see three distinct

bleaches showing the decreased absorbance of the A, B, and C exciton bands. These changes are reversible as evident from the restoration of the spectral features after turning off the light. Similar changes in the exciton spectral features in MoS_2 films have also been observed under the application of electrochemical bias. 30,31

The excitonic bands are sensitive to changes in the band structure, phase transition, and weakened van der Waal interactions due to intercalation of cations. For example, He et al. attributed the disappearance of the excitonic peaks to the changes in the band structure.³² Additionally, the observed changes in optical properties of MoS₂ may also arise from the phase transition (from semiconducting 2H to metallic 1T) induced by electron accumulation. 33,34 Such transformations are accompanied by significant disappearance in the absorption of A, B, and C excitons as shown by Xiong et al. 35 However, in this study, the semiconducting 2H phase was preserved, as demonstrated by the limited impact on the C exciton peak (420 nm) following photoirradiation (Figure 1C (trace b)). According to theoretical studies, the transition from 2H to 1T phase occurs only when the electron accumulation surpasses a specific threshold, specifically at 0.29 electrons per MoS₂ formula unit.³⁶ Acrivos et al. have reported that the A and B exciton levels disappear in Na-intercalated MoS2 due to the screening of free carriers.³⁷ We suggest that an electron storage followed by charge compensation with cations is responsible for the observed spectral changes in Figure 1C. MoS₂ being a semiconductor undergoes charge separation under photoirradiation. The electrons accumulate within the network of MoS₂ nanosheets as the holes are scavenged away by the isopropanol (IPA; reactions 1 and 3). Alcohols are commonly used as sacrificial donors to capture photogenerated holes, leading to the formation of ethoxy radicals, which subsequently oxidize to produce hydrogen (H_2) and carbon dioxide (CO_2) .

$$MoS_2 + h\nu \rightarrow MoS_2(h + e)$$
 exciton generation (1)

$$MoS_2(h + e) \rightarrow MoS_2$$
 exciton recombination (2)

$$MoS_2(h + e) + IPA \rightarrow MoS_2(e) + IPA^+$$

$$charge separation and stabilization$$
 (3

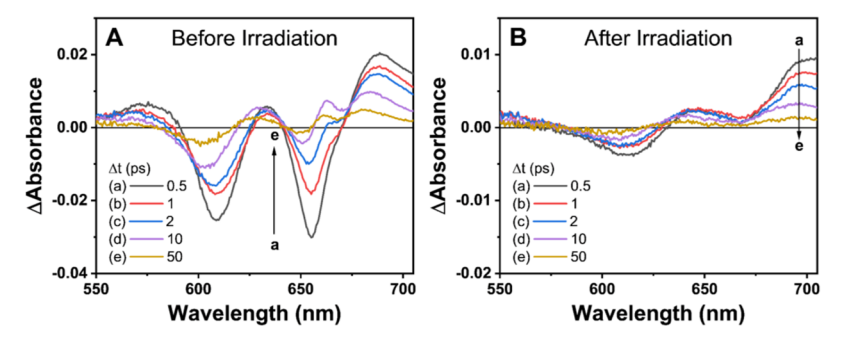


Figure 2. Time-resolved difference absorption spectra recorded following 400 nm laser pulse excitation of (A) preirradiated and (B) postirradiated MoS₂ suspension (deaerated) in IPA. The kinetics of bleach recovery recorded at 610 nm for the two samples are shown in Figure S1.

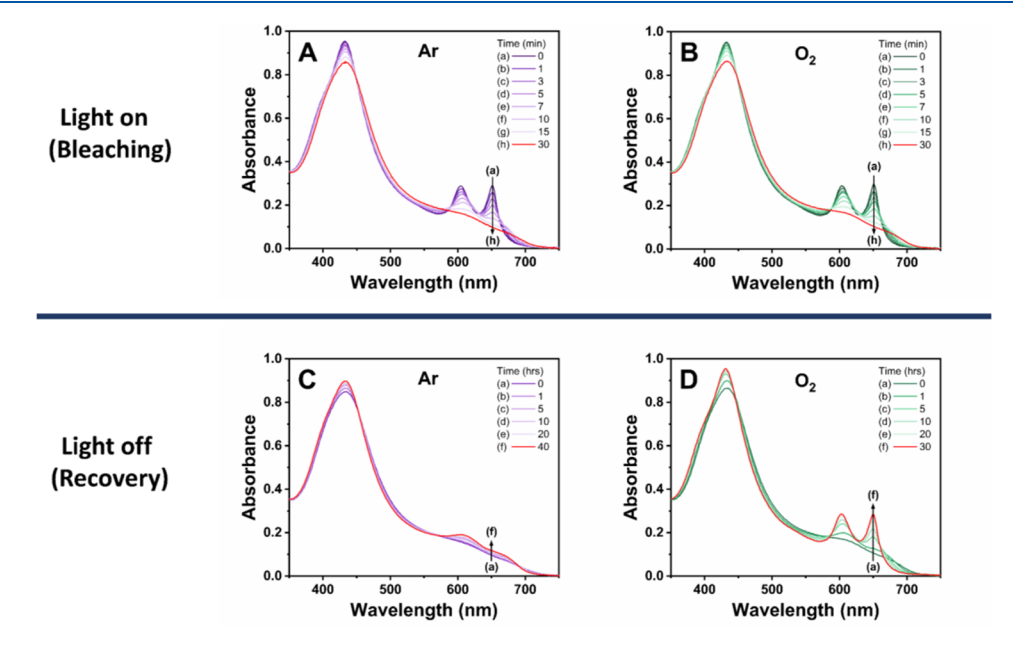


Figure 3. Time-resolved absorption spectra of colloidal MoS_2 nanosheets with white light exposure (top) and subsequent termination of white light (bottom) under different environments. (A) and (C) represent the spectra in an argon inert environment, while (B) and (D) show the spectra in an oxygen environment. The arrows represent the absorbance trends upon white light exposure and termination (light source: $\lambda > 400$ nm, 100 mW/cm²).

It should be noted that this phenomenon of electron accumulation in MoS_2 is typically accompanied by the intercalation of cations to stabilize the stored electrons. Electron storage in 2D suspensions such as graphene oxide has been demonstrated earlier. In the foregoing discussion, we will discuss how the intercalated cations weaken the interlayer interactions, thus, impacting the exciton band features.

The excited states of pre- and postirradiated samples were probed using femtosecond transient absorption spectroscopy under a 400 nm laser pulse excitation. The time-resolved transient absorption (TA) spectra presented in Figure 2 show the influence of photoinduced electron charging effects on the excited state dynamics of MoS_2 nanosheets. In the preirradiated samples, we see prominent bleaching of 655 and 610 nm corresponding to exciton A and B bands, which are corresponding to multilayer MoS_2 . In the postirradiated samples, we do not see bleaching of exciton A band and only a small bleach in the exciton B band. As shown in the steady-state absorption spectra in Figure 1C, the absorption bands corresponding to the A and B excitons are significantly dampened in the postirradiated samples, which is consistent

with the spectra observed from our previous work for the fewlayer colloidal MoS₂. 12 This difference in the steady-state spectral feature is reflected in the transient absorption spectra, with dampening of the A and B exciton bleaches and the dominance of induced absorption in the postirradiated samples. As previously demonstrated through the comparison of transient spectra between multilayer and few-layer MoS₂, ¹² the significant decrease in the bleaches of A and B exciton indicates few-layer MoS₂ features in the postirradiated samples. As discussed in the previous section, electron charging within MoS₂ nanosheets and intercalation of charge compensating cations weakens the interlayer interactions, and these nanosheets behave like individual sheets. We also tracked the recovery of the excited state by monitoring the bleach recovery at 610 nm (Figure S1). A fast decay with a lifetime of 1 ps or less dominates in both samples. Only a small fraction of the excited state results in the charge separation, as evident from the longer tail of bleach recovery. The charge separated pair eventually follows the reaction pathways indicated in reactions 1 and 3.

We compared the evolution of absorption spectra of colloidal MoS_2 nanosheets under oxygen and inert environ-

ments for both light-on (photoirradiation) and light-off (dark) conditions (Figure 3). The two colloidal MoS₂ samples were bubbled with argon and oxygen followed by exposure to white light. Absorption spectra recorded after 30 min of irradiation (Figure 3A,B) showed a decrease in the excitonic peaks similar to the one shown in Figure 1C. The presence of O₂ had minimal influence on the exciton peak decrease as long as we kept the samples under light irradiation. Once the light was turned off, we could see the effect of O₂ (Figure 3C,D). Whereas the excitonic peaks disappeared quickly under light irradiation, the recovery is much longer in dark (minutes vs hours), indicating stabilization of stored electrons. The excitonic peaks in oxygen saturated solution fully recovered after 30 h of storage, while those of the sample under argon barely recovered after 40 h of storage. It should be noted that the time scale of dark recovery even in the presence of oxygen is rather slow showing the sluggish response toward O_2 .

We tracked the kinetics of storage and discharge of stored electrons by monitoring the absorption changes of the A exciton band at 651 nm (Figure 4). The absorption-time

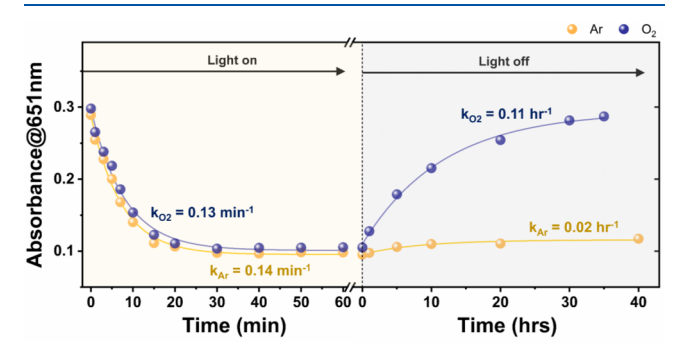


Figure 4. Evolution of the absorption spectra at 651 nm of colloidal MoS₂ nanosheets under irradiation and their recovery upon stopping the irradiation in different environments. Both samples exhibit peak bleaching with no significant difference upon white light irradiation. Regarding the dark recovery, colloidal MoS₂ in oxygen almost fully recovers, while colloidal MoS₂ in argon shows a minimal recovery.

profiles were analyzed with a monoexponential kinetic fit. The rate constants for the bleaching of the exciton band under white light irradiation in both oxygen and argon environments were similar (0.13–0.14 min⁻¹). However, the rate constant for the dark recovery in argon environments is significantly

lower (0.02 h^{-1}) compared to that of oxygen (0.11 h^{-1}) . Previous studies from our group have shown that photogenerated electrons from TiO_2 can be scavenged by oxygen, 43,44 leading to the generation of reduced oxygen species. Therefore, in this study, the observed recovery of the excitonic peaks in the presence of oxygen can be attributed to the extraction of electrons in MoS_2 by oxygen. The difference in recovery kinetics is direct evidence of electron accumulation in MoS_2 upon photoirradiation. This ability of MoS_2 nanosheets to accumulate and stabilize photogenerated electrons offers a potential pathway for energy conversion applications.

To estimate the overall accumulated electrons in MoS_2 after white light irradiation, we utilized ferrocenium (Fc⁺) as an electron acceptor. Fc⁺ is stable under inert atmosphere and transforms to ferrocene (Fc⁰) upon its reduction (Fc⁺/Fc, E^0 = 0.40 V vs SCE).⁴⁵

$$MoS_2(e) + Fc^+(blue) \rightarrow MoS_2 + Fc^0$$
 (yellow) (4)

Earlier studies have demonstrated the utilization of ferrocenium to probe electron transfer at the semiconductor and metal nanoparticle interface. Therefore, by introducing Fc^+ into the postirradiated MoS_2 suspension, we suggest that the stored electrons would transfer from MoS_2 to Fc^+ , leading to the subsequent recovery of the excitonic peaks. A similar concept was validated through the use of Ag^+ . We also tested electron scavenging effect by adding Ag^+ solution to the postirradiated MoS_2 suspension. The solution quickly turned from brown to green as the stored electrons were scavenged away by Ag^+ . The immediate restoration of excitonic peaks upon addition of Ag^+ ions are shown in Figure S2. Details on the Ag^+ reduction in photoirradiated MoS_2 suspension has been presented in our earlier studies. 12

Figure 5A shows the absorption spectra of stock solutions (1 mM) of Fc^+ , Fc^0 , and MoS_2 nanosheet suspensions. Considering that both ferrocenium and ferrocene have low absorbance at 651 nm at micromolar concentrations (close to the A exciton peak), with the negligible amounts required for the titration, we can selectively track the change in the absorption in response to Fc^+ addition. The number of stored electrons scavenged by Fc^+ was estimated by tracking bleach recovery at this wavelength. Similar titration of electrons stored in carbon nanotubes and graphene oxide were conducted using other electron acceptors. A7,48 Both the ferrocenium solution and colloidal MoS_2 were bubbled with argon to purge out oxygen. Colloidal MoS_2 in a sealed quartz cuvette was

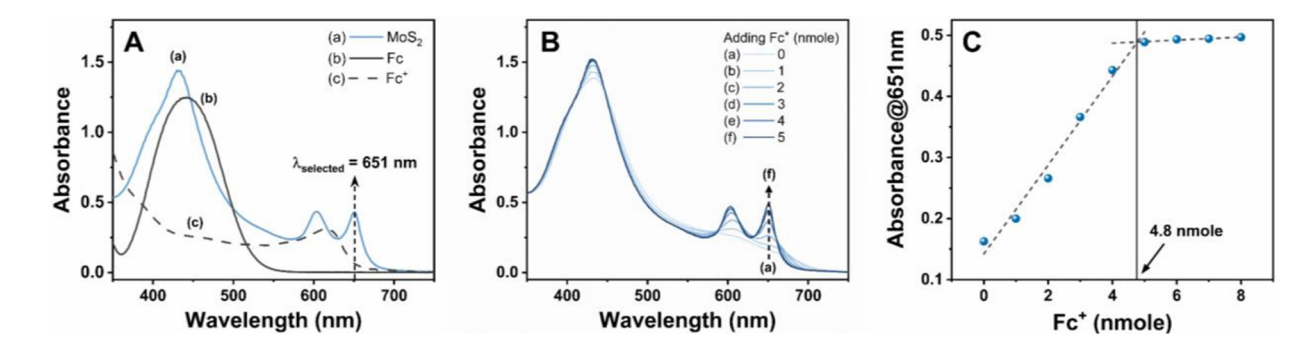


Figure 5. (A) Absorption spectra of deaerated MoS_2 nanosheet suspensions (trace a) in IPA, and ferrocene (1 mM, trace b) and ferrocenium ion (1 mM, trace c) in acetonitrile. (B) Absorption spectra of deaerated colloidal MoS_2 nanosheet suspensions (24 nmol) in IPA after white light exposure, followed by the addition of varying amounts of ferrocenium solution (the total volume was 3 mL). The arrow represents the absorbance trends upon the addition of ferrocenium ions. (C) The corresponding evolution of absorbance monitored at 651 nm with the addition of varying concentrations of ferrocenium ion.

irradiated with white light, and the absorption spectrum was recorded. Small aliquots of known concentration of Fc⁺ were then introduced, and an absorption spectrum was recorded after each addition. The addition of Fc⁺ continued, until there were no further changes in the absorption. The observed changes in the absorbance (651 nm) of photoexcited MoS₂ upon addition of Fc⁺ is shown in Figure 5B. With increasing concentration of Fc⁺, the absorption of A, B, and C exciton peaks recovered in a fashion similar to what we observed in the dark recovery experiment (Figure 3D). This further corroborates the presence of accumulated photogenerated electrons in MoS₂ nanosheets, influencing the exciton spectral features.

We monitored the appearance of MoS_2 exciton bands in response to the addition of Fc^+ by recording the absorbance change at 651 nm corresponding to the A exciton band (Figure 5C). The Fc^+ concentration where the absorbance of MoS_2 at 651 nm attains a plateau is the end point of the titration and corresponds to the concentration of the stored electrons. This value corresponds to 4.8 nmol of stored electrons or ca. 0.2 electrons per MoS_2 formula unit. The number of the stored electrons is below the threshold of 0.29 electrons per MoS_2 unit to observe the 2H to 1T phase transition, 36 thus, confirming the perseverance of the semiconducting 2H phase in these experiments. The findings here indicate the successful utilization of Fc^+ (as an electron acceptor) in capturing photogenerated electrons from colloidal MoS_2 nanosheet suspensions.

Raman spectroscopy is a widely employed technique for determining the number of layers and crystal phases of 2D materials. ^{49–51} For MoS₂, the E_{2g} (in-plane Raman mode) and A_{1g} (out-of-plane Raman mode) are the diagnostic Raman modes used as an indicator of the number of layers by measuring the difference in their frequencies. 50,51 Typically, when the frequency difference is between 18 and 20 cm⁻¹, the MoS₂ flake is a monolayer, while a frequency difference of 20-22 cm⁻¹ corresponds to a bilayer MoS₂, and a frequency difference greater than 23 cm⁻¹ indicates a tri- or multilayer MoS₂. 50,51 Additionally, the unique crystal structures of the two phases of MoS₂ result in different Raman features.⁵² Hence, we utilized a home-built Raman microscope⁵³ to monitor the number of layers and the phase of the colloidal MoS₂ sample before and after white light irradiation (Figure 6). It is important to note that the solvent control experiment, i.e., without MoS₂, indicates that there is no solvent interference in the region of the E_{2g} and A_{1g} peaks.

The sample before irradiation (Figure 6) exhibits the two Raman E_{2g} and A_{1g} signals at approximately 385 and 406 cm⁻¹, respectively, with a frequency difference of 21 cm⁻¹, which corresponds to a few-layer MoS₂.⁵⁴ For the sample after irradiation, the E_{2g} mode remains almost unchanged in the peak position, while the A_{1g} peak splits and is suppressed in intensity. Note that the MoS2 sample was subjected to a white light irradiation for 30 min before taking the measurements. By analyzing the Raman spectra with multipeak fitting, we identified three peaks labeled as E_{2g} , A_{1g} , and A_{1g} , with peak positions at approximately 385, 400, and 407 cm⁻¹, respectively. Intriguingly, the frequency difference between E_{2g} and A_{1g}^* is 15 cm⁻¹, which is significantly lower than the frequency difference of the E_{2g} and A_{1g} peaks of monolayer MoS_2 . This implies that the photoinduced A_{1g}^* mode does not arise from changes in the number of layers. It should be noted that the photoinduced A_{1g}^* mode can also undergo dark recovery to the original peak position and intensity. Recently,

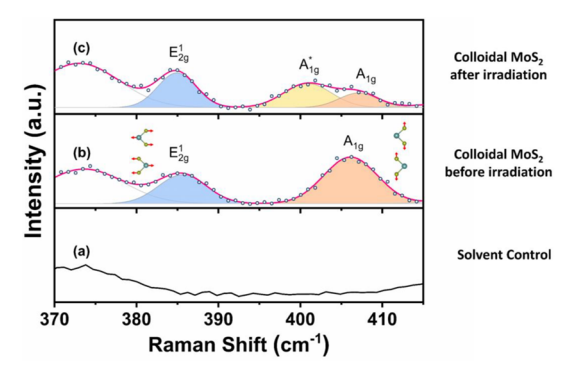


Figure 6. Raman spectra of (a) PVP/IPA solvent and colloidal MoS₂ nanosheets (b) before and (c) after white light irradiation. Following white light irradiation, the A_{1g} peak splits and red-shifts, denoted as A_{1g}^* . The inset displays the vibrational modes of E^1_{2g} and A_{1g} of MoS₂. PVP/IPA solvent serves as the background (excitation wavelength = 532 nm)

Sun et al. observed an emergence of A_{1g}^* mode in cetyltrimethylammonium cations (CTA⁺) intercalated MoS₂. From their polarized and temperature-dependent Raman measurements, they concluded that the A_{1g}^* peak results from a similar vibration mode as the A_{1g} peak, suggesting CTA⁺ intercalation and electron doping. Thus, in the current study, the emergence of the A_{1g}^* mode could be rationalized by the intercalation of counterions, which is essential for charge compensation to maintain overall neutrality, especially in the presence of photogenerated electrons accumulation. These counterions originate from THA⁺, used during the sample preparation step. A more comprehensive investigation on the role of different cations in charge stabilization is currently underway.

To gain additional insights into the impact of photogenerated electron accumulation on the colloidal MoS2 sample, zeta potential and dynamic light scattering (DLS) measurements were conducted to evaluate the overall charge and size, before and after white light irradiation, as shown in Figure S3. The zeta potential decreased from -65.7 to -46.9 mV as we subjected the MoS₂ suspension to photoirradiation (Figure S3a). During the same period, size measurements conducted via DLS revealed an increase in the effective size from 74.2 to 94.4 nm (Figure S3b). The decrease in zeta potential could be attributed to two major factors: (1) particle aggregation and (2) counterion intercalation. However, according to Raman measurements (vide supra), we did not observe a substantial increase in the frequency difference between the E_{2g} and A_{1g} peaks after irradiation, thus ruling out any increase in the number of layers-particle aggregation. By considering the emergence of the A_{1g}^* Raman mode upon irradiation, we conclude that the colloidal MoS₂ undergoes counterion intercalation to maintain the overall charge balance, resulting in the decrease of the Zeta potential. The increase in size (Figure S3b) also supports the proposed intercalation of the counterions within the MoS₂ lattice. It is worth noting that the zeta potential measurements show that the colloidal MoS₂ nanosheets before or after irradiation are both negatively charged, ranging from -70 to -50 mV, thus rendering excellent colloidal stability in polar solvents.

Further experiments to investigate the photoinduced counterion intercalation were conducted using MoS_2 films. Postirradiated (100 mW/cm², 30 min) colloidal MoS_2 suspension was drop-cast immediately onto a microscope

Scheme 1. Schematic Illustration of Colloidal MoS₂ Nanosheets Undergoing Counter Ion Intercalation upon White Light Exposure and Its Decay Process (Light Off)^a



^aCounter ion: THA⁺.

slide and left to air-dry. Remarkably, the postirradiated sample did not undergo dark recovery, and the brown color persisted for days without any noticeable changes (Figure S4). Similarly, the nonirradiated film maintained its green color. To obtain more insights into the origin of this peculiar behavior of MoS₂ films, we performed Raman spectroscopy of the films, as shown in Figure S4. The film containing nonirradiated MoS₂ (green) exhibits the E_{2g} and A_{1g} modes located at approximately 382 and 408 cm⁻¹, respectively, with a frequency difference of 26 cm⁻¹. The increase in the peak spacing indicates the formation of multilayer MoS₂. However, for the film with irradiated MoS₂ (brown), the $A_{1\sigma}$ mode was highly suppressed and the $A_{1\sigma}$ mode became prominent. The difference in the extent of A_{1g} to A_{1g}^* conversion, between the MoS₂ dispersion and films, can be attributed by the change in the experimental conditions. The persistence of the brown color and A_{1g}^* peak in film with irradiated MoS₂ further points to the counterion intercalation of MoS₂. In the case of colloidal MoS₂, dark recovery was likely made possible by the solvent system, as the charge compensating ions can freely move. Further close analysis of the 100-350 cm⁻¹ region in the Raman spectra of the respective MoS₂ films revealed the absence of any characteristic Raman modes associated with the 1T-MoS₂ phase. This observation further corroborates the preservation of semiconducting 2H-MoS₂ before and after photogenerated electron accumulation.

It is evident that photoexcitation of MoS₂ induces the generation and subsequent accumulation of electrons. We propose that upon photoexcitation of colloidal MoS₂, the holes are scavenged by IPA leading to the accumulation of electrons. These accumulated electrons induce changes in the optical properties of MoS2; color changes from green to brown as the absorption of the A and B excitonic peaks decrease (Scheme 1). In order to maintain the overall charge balance, the positive counterions are consequently intercalated within the MoS₂ lattice, as shown in Scheme 1. In the presence of a solvent, the intercalated counterions are expelled when the accumulated electrons are scavenged by oxygen or Fc⁺. In films, however, the intercalated ions remain entrapped, thus stabilizing the accumulated electrons. Counter ion intercalation to stabilize injected electrons which usually reduces the metal ions to lower valence state is seen for metal oxides (e.g., stabilization of Ti^{3+} states in TiO_2). 56-58

Based on the results from the environment-dependent experiments, Raman spectroscopy, and zeta potential measurements, we propose an underlying mechanism for photogenerated electron accumulation in colloidal MoS₂, as illustrated in Scheme 1. Upon exposure to white light, photogenerated electrons accumulate in colloidal MoS₂, with

counterions intercalating within the MoS_2 lattice to maintain charge balance. The system undergoes dark recovery when the light is cut off. Photoinduced electron accumulation induces changes in the optical properties of MoS_2 without undergoing a phase transition, as the interlayer interaction is minimized. The control experiments with solid-state samples imply that counterion intercalation plays an essential role in stabilizing the photogenerated electrons.

ASSOCIATED CONTENT

Supporting Information

The Supporting Information is available free of charge at https://pubs.acs.org/doi/10.1021/acs.jpclett.4c00454.

Synthesis of MoS₂ through electrochemical intercalation; Sample characterization; Zeta potential; Dynamic light scattering measurements (PDF)

AUTHOR INFORMATION

Corresponding Author

Prashant V. Kamat — Radiation Laboratory, Department of Chemistry and Biochemistry, and Department of Chemical and Biomolecular Engineering, University of Notre Dame, Notre Dame, Indiana 46556, United States; ocid.org/0000-0002-2465-6819; Email: pkamat@nd.edu

Authors

Bo-An Chen — Radiation Laboratory and Department of Chemistry and Biochemistry, University of Notre Dame, Notre Dame, Indiana 46556, United States; ⊚ orcid.org/ 0000-0001-5778-027X

Nathaniel L. Dominique — Department of Chemistry and Biochemistry, University of Notre Dame, Notre Dame, Indiana 46556, United States; orcid.org/0000-0002-0439-9982

Anthony Kipkorir — Radiation Laboratory and Department of Chemistry and Biochemistry, University of Notre Dame, Notre Dame, Indiana 46556, United States; ocid.org/0000-0003-0417-2478

Jon P. Camden – Department of Chemistry and Biochemistry, University of Notre Dame, Notre Dame, Indiana 46556, United States; orcid.org/0000-0002-6179-2692

Sylwia Ptasinska – Radiation Laboratory and Department of Physics and Astronomy, University of Notre Dame, Notre Dame, Indiana 46S56, United States; orcid.org/0000-0002-7550-8189

Complete contact information is available at: https://pubs.acs.org/10.1021/acs.jpclett.4c00454

Notes

The authors declare no competing financial interest.

ACKNOWLEDGMENTS

The research work is supported by the Division of Chemical Sciences, Geosciences, and Biosciences, Office of Basic Energy Sciences of the U.S. Department of Energy (B.C., A.K., P.K., and S.P., Award DE-FC02-04ER15533) and the National Science Foundation (J.P.C. and N.L.D., Award CHE-2108330). Any opinions, findings, and conclusions expressed in this material are those of the authors and do not necessarily reflect the views of the National Science Foundation or U.S. Department of Energy. The authors thank the Notre Dame Integrated Imaging Facility for using the TEM and Material Characterization Facility for recording Raman spectra. The authors also acknowledge the University of Notre Dame Equipment Restoration and Renewal program for purchasing the Spectra Physics laser used for the transient absorption measurements. This is contribution number NDRL No. 5425 from the Notre Dame Radiation Laboratory.

REFERENCES

- (1) Chhowalla, M.; Shin, H. S.; Eda, G.; Li, L.-J.; Loh, K. P.; Zhang, H. The Chemistry of Two-dimensional Layered Transition Metal Dichalcogenide Nanosheets. *Nat. Chem.* **2013**, *5* (4), 263–275.
- (2) Novoselov, K. S.; Mishchenko, A.; Carvalho, A.; Castro Neto, A. H. 2D Materials and van der Waals Heterostructures. *Science* **2016**, 353 (6298), aac9439.
- (3) Manzeli, S.; Ovchinnikov, D.; Pasquier, D.; Yazyev, O. V.; Kis, A. 2D Transition Metal Dichalcogenides. *Nat. Rev. Mater.* **2017**, 2 (8), na.
- (4) Radisavljevic, B.; Radenovic, A.; Brivio, J.; Giacometti, V.; Kis, A. Single-layer MoS₂ Transistors. *Nat. Nanotechnol.* **2011**, *6* (3), 147–150.
- (5) Yin, Z.; Li, H.; Li, H.; Jiang, L.; Shi, Y.; Sun, Y.; Lu, G.; Zhang, Q.; Chen, X.; Zhang, H. Single-Layer MoS₂ Phototransistors. *ACS Nano* **2012**, *6* (1), 74–80.
- (6) Lopez-Sanchez, O.; Lembke, D.; Kayci, M.; Radenovic, A.; Kis, A. Ultrasensitive Photodetectors Based on Monolayer MoS₂. *Nat. Nanotechnol.* **2013**, *8* (7), 497–501.
- (7) Cheng, R.; Li, D.; Zhou, H.; Wang, C.; Yin, A.; Jiang, S.; Liu, Y.; Chen, Y.; Huang, Y.; Duan, X. Electroluminescence and Photocurrent Generation from Atomically Sharp WSe₂/MoS₂ Heterojunction p—n Diodes. *Nano Lett.* **2014**, *14* (10), 5590–5597.
- (8) Withers, F.; Del Pozo-Zamudio, O.; Mishchenko, A.; Rooney, A. P.; Gholinia, A.; Watanabe, K.; Taniguchi, T.; Haigh, S. J.; Geim, A. K.; Tartakovskii, A. I.; et al. Light-emitting Diodes by Band-structure Engineering in van der Waals Heterostructures. *Nat. Mater.* **2015**, *14* (3), 301–306.
- (9) Mak, K. F.; Lee, C.; Hone, J.; Shan, J.; Heinz, T. F. Atomically Thin MoS_2 : A New Direct-gap Semiconductor. *Phys. Rev. Lett.* **2010**, 105 (13), 136805.
- (10) Kuc, A.; Zibouche, N.; Heine, T. Influence of Quantum Confinement on the Electronic Structure of the Transition Metal Sulfide TS₂. *Phys. Rev. B* **2011**, 83 (24), 245213.
- (11) Cho, J.; Suwandaratne, N. S.; Razek, S.; Choi, Y.-H.; Piper, L. F. J.; Watson, D. F.; Banerjee, S. Elucidating the Mechanistic Origins of Photocatalytic Hydrogen Evolution Mediated by MoS₂/CdS Quantum-Dot Heterostructures. *ACS Appl. Mater. Interfaces* **2020**, 12 (39), 43728–43740.
- (12) Chen, B.-A.; Ptasinska, S.; Kamat, P. V. Metal Cocatalyst Dictates Electron Transfer in Ag-Decorated MoS₂ Nanosheets. *J. Phys. Chem. C* **2022**, *126* (29), 11907–11914.
- (13) Wang, W.; Song, Y.; Ke, C.; Li, Y.; Liu, Y.; Ma, C.; Wu, Z.; Qi, J.; Bao, K.; Wang, L.; et al. Filling the Gap between Heteroatom Doping and Edge Enrichment of 2D Electrocatalysts for Enhanced Hydrogen Evolution. ACS Nano 2023, 17 (2), 1287–1297.

- (14) Zong, X.; Wu, G.; Yan, H.; Ma, G.; Shi, J.; Wen, F.; Wang, L.; Li, C. Photocatalytic H₂ Evolution on MoS₂/CdS Catalysts under Visible Light Irradiation. *J. Phys. Chem. C* **2010**, *114* (4), 1963–1968.
- (15) Coleman, J. N.; Lotya, M.; O'Neill, A.; Bergin, S. D.; King, P. J.; Khan, U.; Young, K.; Gaucher, A.; De, S.; Smith, R. J.; et al. Two-Dimensional Nanosheets Produced by Liquid Exfoliation of Layered Materials. *Science* **2011**, *331* (6017), 568–571.
- (16) Zeng, Z.; Yin, Z.; Huang, X.; Li, H.; He, Q.; Lu, G.; Boey, F.; Zhang, H. Single-Layer Semiconducting Nanosheets: High-Yield Preparation and Device Fabrication. *Angew. Chem., Int. Ed.* **2011**, *50* (47), 11093–11097.
- (17) Nicolosi, V.; Chhowalla, M.; Kanatzidis, M. G.; Strano, M. S.; Coleman, J. N. Liquid Exfoliation of Layered Materials. *Science* **2013**, 340 (6139), 1226419.
- (18) Zhang, X.; Lai, Z.; Tan, C.; Zhang, H. Solution-Processed Two-Dimensional MoS₂ Nanosheets: Preparation, Hybridization, and Applications. *Angew. Chem., Int. Ed.* **2016**, *55* (31), 8816–8838.
- (19) Pinilla, S.; Coelho, J.; Li, K.; Liu, J.; Nicolosi, V. Two-dimensional Material Inks. *Nat. Rev. Mater.* **2022**, 7 (9), 717–735.
- (20) Yang, R.; Fan, Y.; Mei, L.; Shin, H. S.; Voiry, D.; Lu, Q.; Li, J.; Zeng, Z. Synthesis of Atomically Thin Sheets by the Intercalation-based Exfoliation of Layered Materials. *Nat. Synth.* **2023**, 2 (2), 101–118.
- (21) Lin, Z.; Liu, Y.; Halim, U.; Ding, M.; Liu, Y.; Wang, Y.; Jia, C.; Chen, P.; Duan, X.; Wang, C.; et al. Solution-processable 2D Semiconductors for High-performance Large-area Electronics. *Nature* **2018**, *562* (7726), 254–258.
- (22) Kuo, L.; Sangwan, V. K.; Rangnekar, S. V.; Chu, T.-C.; Lam, D.; Zhu, Z.; Richter, L. J.; Li, R.; Szydłowska, B. M.; Downing, J. R.; et al. All-Printed Ultrahigh-Responsivity MoS₂ Nanosheet Photodetectors Enabled by Megasonic Exfoliation. *Adv. Mater.* **2022**, 34 (34), 2203772.
- (23) Chen, M.; Cui, D.; Wang, N.; Weng, S.; Zhao, Z.; Tian, F.; Gao, X.; He, K.; Chiang, C.-T.; Albawardi, S.; et al. Inkjet-Printed MoS₂ Nanoplates on Flexible Substrates for High-Performance Field Effect Transistors and Gas Sensing Applications. *ACS Appl. Nano Mater.* **2023**, *6* (5), 3236–3244.
- (24) Tsai, M.-L.; Su, S.-H.; Chang, J.-K.; Tsai, D.-S.; Chen, C.-H.; Wu, C.-I.; Li, L.-J.; Chen, L.-J.; He, J.-H. Monolayer MoS_2 Heterojunction Solar Cells. *ACS Nano* **2014**, *8* (8), 8317–8322.
- (25) Thurston, T. R.; Wilcoxon, J. P. Photooxidation of Organic Chemicals Catalyzed by Nanoscale MoS₂. *J. Phys. Chem. B* **1999**, *103* (1), 11–17.
- (26) Yu, X.; Rahmanudin, A.; Jeanbourquin, X. A.; Tsokkou, D.; Guijarro, N.; Banerji, N.; Sivula, K. Hybrid Heterojunctions of Solution-Processed Semiconducting 2D Transition Metal Dichalcogenides. ACS Energy Lett. 2017, 2 (2), 524–531.
- (27) Splendiani, A.; Sun, L.; Zhang, Y.; Li, T.; Kim, J.; Chim, C.-Y.; Galli, G.; Wang, F. Emerging Photoluminescence in Monolayer MoS₂. *Nano Lett.* **2010**, *10* (4), 1271–1275.
- (28) Hill, H. M.; Rigosi, A. F.; Roquelet, C.; Chernikov, A.; Berkelbach, T. C.; Reichman, D. R.; Hybertsen, M. S.; Brus, L. E.; Heinz, T. F. Observation of Excitonic Rydberg States in Monolayer MoS₂ and WS₂ by Photoluminescence Excitation Spectroscopy. *Nano Lett.* **2015**, *15* (5), 2992–2997.
- (29) Carvalho, A.; Ribeiro, R. M.; Castro Neto, A. H. Band Nesting and the Optical Response of Two-dimensional Semiconducting Transition Metal Dichalcogenides. *Phys. Rev. B* **2013**, 88 (11), na.
- (30) Almaraz, R.; Sayer, T.; Toole, J.; Austin, R.; Farah, Y.; Trainor, N.; Redwing, J. M.; Krummel, A.; Montoya-Castillo, A.; Sambur, J. Quantifying Interfacial Energetics of 2D Semiconductor Electrodes using in situ Spectroelectrochemistry and Many-body theory. *Energy Environ. Sci.* **2023**, *16* (10), 4522–4529.
- (31) Wurst, K. M.; Strolka, O.; Hiller, J.; Keck, J.; Meixner, A. J.; Lauth, J.; Scheele, M. Electronic Structure of Colloidal 2H-MoS₂ Mono and Bilayers Determined by Spectroelectrochemistry. *Small* **2023**, *19* (23), 2207101.
- (32) He, Q.; Lin, Z.; Ding, M.; Yin, A.; Halim, U.; Wang, C.; Liu, Y.; Cheng, H.-C.; Huang, Y.; Duan, X. In Situ Probing Molecular

- Intercalation in Two-Dimensional Layered Semiconductors. *Nano Lett.* **2019**, *19* (10), 6819–6826.
- (33) Ambrosi, A.; Sofer, Z.; Pumera, M. Lithium Intercalation Compound Dramatically Influences the Electrochemical Properties of Exfoliated MoS₂. *Small* **2015**, *11* (5), 605–612.
- (34) Tan, S. J. R.; Abdelwahab, I.; Ding, Z.; Zhao, X.; Yang, T.; Loke, G. Z. J.; Lin, H.; Verzhbitskiy, I.; Poh, S. M.; Xu, H.; et al. Chemical Stabilization of 1T' Phase Transition Metal Dichalcogenides with Giant Optical Kerr Nonlinearity. *J. Am. Chem. Soc.* **2017**, 139 (6), 2504–2511.
- (35) Xiong, F.; Wang, H.; Liu, X.; Sun, J.; Brongersma, M.; Pop, E.; Cui, Y. Li Intercalation in MoS_2 : In Situ Observation of Its Dynamics and Tuning Optical and Electrical Properties. *Nano Lett.* **2015**, *15* (10), 6777–6784.
- (36) Li, Y.; Duerloo, K.-A. N.; Wauson, K.; Reed, E. J. Structural Semiconductor-to-semimetal Phase Transition in Two-dimensional Materials Induced by Electrostatic Gating. *Nat. Commun.* **2016**, *7* (1), 10671
- (37) Acrivos, J. V.; Liang, W. Y.; Wilson, J. A.; Yoffe, A. D. Optical Studies of Metal-semiconductor Transmutations Produced by Intercalation. *J. Phys. C: Solid State Phys.* **1971**, 4 (1), L18.
- (38) Schneider, J.; Bahnemann, D. W. Undesired Role of Sacrificial Reagents in Photocatalysis. *J. Phys. Chem. Lett.* **2013**, 4 (20), 3479–3483.
- (39) Yu, Y.; Kipkorir, A.; Choi, M. Y.; Kamat, P. V. Photocatalytic Membrane for Hydrogen Evolution: Directed Electron and Hole Transfer across Pt–AgInS₂–Nafion. *ACS Mater. Lett.* **2024**, 1856–1862.
- (40) Yu, Y.; Kipkorir, A.; Choi, M. Y.; Kamat, P. V. Directional Electron Transfer across In₂S₃/ZnS-Embedded Photocatalytic Membranes. *ACS Appl. Energy Mater.* **2024**, 7 (2), 681–688.
- (41) Radich, E. J.; Kamat, P. V. Origin of Reduced Graphene Oxide Enhancements in Electrochemical Energy Storage. *ACS Catal.* **2012**, *2* (5), 807–816.
- (42) Lightcap, I. V.; Kamat, P. V. Graphitic Design: Prospects of Graphene-Based Nanocomposites for Solar Energy Conversion, Storage, and Sensing. *Acc. Chem. Res.* **2013**, *46* (10), 2235–2243.
- (43) Scheidt, R. A.; Kerns, E.; Kamat, P. V. Interfacial Charge Transfer between Excited CsPbBr₃ Nanocrystals and TiO₂: Charge Injection versus Photodegradation. *J. Phys. Chem. Lett.* **2018**, 9 (20), 5962–5969.
- (44) DuBose, J. T.; Kamat, P. V. TiO₂-Assisted Halide Ion Segregation in Mixed Halide Perovskite Films. *J. Am. Chem. Soc.* **2020**, *142* (11), 5362–5370.
- (45) Paul, A.; Borrelli, R.; Bouyanfif, H.; Gottis, S.; Sauvage, F. Tunable Redox Potential, Optical Properties, and Enhanced Stability of Modified Ferrocene-Based Complexes. *ACS Omega* **2019**, *4* (12), 14780–14789.
- (46) DuBose, J. T.; Kamat, P. V. Probing Perovskite Photocatalysis. Interfacial Electron Transfer between CsPbBr₃ and Ferrocene Redox Couple. *J. Phys. Chem. Lett.* **2019**, *10* (20), 6074–6080.
- (47) Kongkanand, A.; Kamat, P. V. Interactions of Single Wall Carbon Nanotubes with Methyl Viologen Radicals. Quantitative Estimation of Stored Electrons. *J. Phys. Chem. C* **2007**, *111* (26), 9012–9015.
- (48) Krishnamurthy, S.; Lightcap, I. V.; Kamat, P. V. Electron Transfer Between Methyl Viologen Radicals and Graphene Oxide: Reduction, Electron Storage and Discharge. *J. Photochem. Photobiol., A* **2011**, 221 (2), 214–219.
- (49) Jiménez Sandoval, S.; Yang, D.; Frindt, R. F.; Irwin, J. C. Raman Study and Lattice Dynamics of Single Molecular Layers of MoS₂. *Phys. Rev. B Condens.* **1991**, *44* (8), 3955–3962.
- (50) Lee, C.; Yan, H.; Brus, L. E.; Heinz, T. F.; Hone, J.; Ryu, S. Anomalous Lattice Vibrations of Single- and Few-Layer MoS₂. ACS Nano **2010**, 4 (5), 2695–2700.
- (51) Li, H.; Zhang, Q.; Yap, C. C. R.; Tay, B. K.; Edwin, T. H. T.; Olivier, A.; Baillargeat, D. From Bulk to Monolayer MoS₂: Evolution of Raman Scattering. *Adv. Funct. Mater.* **2012**, 22 (7), 1385–1390.

- (52) Liu, L.; Wu, J.; Wu, L.; Ye, M.; Liu, X.; Wang, Q.; Hou, S.; Lu, P.; Sun, L.; Zheng, J.; et al. Phase-selective Synthesis of 1T' MoS₂ Monolayers and Heterophase Bilayers. *Nat. Mater.* **2018**, *17* (12), 1108–1114.
- (53) Demille, T. B.; Hughes, R. A.; Dominique, N.; Olson, J. E.; Rouvimov, S.; Camden, J. P.; Neretina, S. Large-area Periodic Arrays of Gold Nanostars Derived from HEPES-, DMF-, and Ascorbic-acid-driven Syntheses. *Nanoscale* **2020**, *12* (31), 16489–16500.
- (54) Li, X.-L.; Han, W.-P.; Wu, J.-B.; Qiao, X.-F.; Zhang, J.; Tan, P.-H. Layer-Number Dependent Optical Properties of 2D Materials and Their Application for Thickness Determination. *Adv. Funct. Mater.* **2017**, *27* (19), 1604468.
- (55) Sun, Y.; Yin, S.; Peng, R.; Liang, J.; Cong, X.; Li, Y.; Li, C.; Wang, B.; Lin, M.-L.; Tan, P.-H.; et al. Abnormal Out-of-Plane Vibrational Raman Mode in Electrochemically Intercalated Multilayer MoS₂. *Nano Lett.* **2023**, 23 (11), 5342–5349.
- (56) Frank, S. N.; Bard, A. J. Semiconductor Electrodes. II. Electrochemistry at n-type Titanium Dioxide Electrodes in Acetonitrile Solutions. *J. Am. Chem. Soc.* **1975**, *97* (26), 7427–7433.
- (57) Ramesha, G. K.; Brennecke, J. F.; Kamat, P. V. Origin of Catalytic Effect in the Reduction of $\rm CO_2$ at Nanostructured $\rm TiO_2$ Films. ACS Catal. **2014**, 4 (9), 3249–3254.
- (58) Zhang, W.; Seo, D.-H.; Chen, T.; Wu, L.; Topsakal, M.; Zhu, Y.; Lu, D.; Ceder, G.; Wang, F. Kinetic Pathways of Ionic Transport in Fast-charging Lithium Titanate. *Science* **2020**, *367* (6481), 1030–1034.